RESEARCH ARTICLE

Compact Slow-Wave Half-Mode Substrate Integrated Waveguide With Spoof Surface Plasmon Polaritons for Miniaturized Microwave Circuits

YUXI LIU[1], **YIMING ZHANG**[2], **HUI LIU**[1,2], **(Member, IEEE)**,
ERIK FORSBERG[3], **(Member, IEEE), YUAN ZHANG**[1],
AND SAILING HE[1,2,4], **(Fellow, IEEE)**

[1]RF Circuit and Microwave System Laboratory, Centre for Optical and Electromagnetic Research, South China Academy of Advanced Optoelectronics, South China Normal University, Guangzhou 510006, China
[2]RF Circuit and Microwave System Laboratory, Center for Optical and Electromagnetic Research, National Engineering Research Center for Optical Instruments, Zhejiang University, Hangzhou 310058, China
[3]Center for Optical and Electromagnetic Research, College of Optical Science and Engineering, Zhejiang University, Hangzhou 310058, China
[4]Department of Electromagnetic Engineering, School of Electrical Engineering, KTH Royal Institute of Technology, 100 44 Stockholm, Sweden

Corresponding author: Sailing He (sailing@kth.se)

ABSTRACT A slow-wave half-mode substrate integrated waveguide with a spoof surface plasmon polariton (SW-HMSIW-SSPP) transmission line structure is proposed, analyzed, and demonstrated. Results show longitudinal and lateral size reductions of more than 80% and 73%, respectively, as compared with an equivalent SIW at the same cutoff frequency while maintaining a low attenuation constant of 0.02 dB/mm. By altering the geometric parameters of the SW-HMSIW-SSPP the dispersion curve can be tailored. The dispersion and electromagnetic (EM) field distribution characteristics of the proposed SW-HMSIW-SSPP unit cell and overall structure are analyzed by HFSS simulations and an equivalent circuit, and pertinent performance parameters are compared to those of SW-HMSIW and HMSIW-SSPP structures. A proof-of-concept PCB SW-HMSIW-SSPP sample was fabricated, and measurement results showing a band-pass of 4.8-11.5 GHz are found consistent with simulation results. The SW-HMSIW-SSPP structure has applications in the design of miniaturized microwave circuits.

INDEX TERMS Metallized blind via-holes, miniaturization, slow-wave effect, spoof surface plasmon polaritons, substrate integrated waveguide.

I. INTRODUCTION

Large-scale application of 5th generation (5G) mobile network communication featuring high frequency and high speed has increased demands for miniaturization of planar circuits employed in microwave and RF systems, requiring

The associate editor coordinating the review of this manuscript and approving it for publication was Nagendra Prasad Pathak.

circuits to have low profile, be lightweight, and able to be fabricated at low cost [1]. Traditional planar transmission lines, such as microstrips [2] and coplanar waveguides [3], have advantages of small size, planar geometry [4], low cost [5], [6] and applicability in a wide range of scenarios. However, such planar transmission lines are semi-open electromagnetic field structures, and thus a source of electromagnetic radiation and leakage that can cause signal integrity

problems such as delay, attenuation, and crosstalk; problems that increases in severity at increasing operating frequencies. For these reasons, substrate integrated waveguides (SIW) [7], [8] are of interest as they can overcome the issues of electromagnetic leakage and signal integrity of semi-open planar transmission lines while retaining their merits. An SIW is formed on a low-loss dielectric substrate covered with metal layers, using two rows of metallized vias that act as the equivalents of the sidewalls of traditional rectangular metal waveguides. As a result, SIWs exhibit the same advantages as those of metal waveguides, i.e., low loss, high Q value, high power capacity, and electromagnetic shielding. However, to ensure effective operation, the width of an SIW structure is designed to be a quarter of the wavelength corresponding to the lowest frequency. The resulting large circuit area of SIWs restricts their use in compact microwave systems at low RF frequencies [9], [10], [11].

Several approaches to develop more compact SIW circuits have been reported. A ridge SIW proposed in [12] achieved a 40% reduction in width compared to a conventional SIW by loading a central row of partial-height metal posts connected at their bottom by a metal. In [13], a half-mode SIW (HMSIW) bisects the SIW along a fictitious quasi-magnetic wall, which reduced the width by 50%. A folded SIW introduced in [14], which folds the SIW along the E-plane, was able to reduce the width by half. These approaches however only address size reduction in the lateral dimension of the waveguide.

Reduction of the transverse SIW dimension is not strictly a size reduction from the point-of-view of component footprint; from that perspective, size reduction in the longitudinal dimension along the direction of wave transmission is of importance to consider. For this purpose, Niembro-Martin et al. proposed the concept of slow-wave (SW) SIWs [15] in which the electric field strength is greatly enhanced without disturbing the magnetic field by loading arrays of metallized blind via-holes inside the SIW. Due to these, the effective permittivity is increased while the effective permeability remains unchanged. Both the cutoff frequency and phase velocity were reduced by 40%, resulting in a reduction of both lateral and longitudinal dimensions. In [16], a slow-wave HMSIW (SW-HMSIW) was proposed, which is achieved by combining a SW-SIW with a HMSIW, which reduced the waveguide width by nearly half compared with the SW-SIW. An slow-wave structure can also be realized by modifying the top metal layer with a periodic microstrip polyline [17] or by using lumped inductors [18]. The SW-SIW introduced in [19] reduced the size of an equivalent SIW by more than 40% in both lateral and longitudinal dimensions by using enhanced capacitance between the signal trace grid and periodic grounded patches on the same top layer. The enhanced SW-SIW in [20] incorporated multi-antipodal metalized blind via-holes and distributed metal strips longitudinally connecting the bottom of upper posts. This SIW-based topology achieved a lateral dimension

reduction of 55.5% and a longitudinal dimension reduction of more than 50% with reference to the conventional SIW with the same lateral size. The SW-SIW in [21] loaded patches that are shorted to the SIW bottom plane by blind via-holes, which simultaneously increased the effective permeability and permittivity resulting in a decrease of the lateral dimension and longitudinal length by 53% and 73%, respectively.

A surface plasmon polariton (SPP) is a unique surface electromagnetic wave that propagates along a metal-air or metal-dielectric interface at optical frequencies [22], which confines light to the interface at a subwavelength scale. However, in the terahertz and microwave bands, metals are regarded as perfect electric conductors and lack the ability to confine electromagnetic fields. Spoof Surface Plasmon Polariton (SSPP) structures, achieved by etching artificial periodic structures, such as a 1-D metal grating or a 2-D metal array, have been proposed to achieve spatial confinement and slow-wave features of SPPs in the microwave spectrum [23], [24], [25], [26]. A prominent advantage of SSPPs is that the dispersion characteristics and spatial confinement can be controlled simply by geometrical means and the longitudinal reduction ability of SSPP structures make them suitable for miniaturization of SIWs. A HMSIW combined with an SSPP structure by etching subwavelength corrugated grooves on the top metal layer of an HMSIW was proposed in [27]. In [28], the slow-wave effect was enhanced in an HMSIW-SSPP by connecting the subwavelength corrugated grooves of the top layer with 1-D periodic patches at the bottom layer through center metalized via-holes. A ridged HMSIW (RHMSIW) combined with SSPP, which reduced the longitudinal size by over 50% and the lateral width by 70% as compared to a conventional SIW, was reported in [29]. Motivated by the ability to reduce size by using SSPP structures, devices such as on-chip bandpass filter (BPF) [30] and diplexer [31] based on SSPP structures have been designed and investigated.

However, approaches to miniaturization reported to date have not been able to achieve significant simultaneous size reduction of the longitudinal and the transverse dimensions. We note that SW-SIW and SSPP structures can be utilized to obtain significant SIW lateral and longitudinal size reductions, however no study on whether these two methods can be effectively combined to obtain a more compact SIW have been reported and there is still a general lack of studies on the characteristics of the combination of these two methods in the literature. This paper's aim is to do so and we propose and investigate a slow-wave half-mode substrate integrated waveguide with spoof surface plasmon polaritons (SW-HMSIW-SSPP). The SW-HMSIW-SSPP combines the convenience of an SW-HMSIW for integration with other slow-wave structures and the ability of SSPPs to tailor dispersion by adjustment of geometric parameters, enabling significant miniaturization in both longitudinal and lateral directions. An SW-HMSIW with an array of metallized blind via-holes inside the HMSIW increases the effective

permittivity, which reduces the cutoff frequency and phase velocity. An SSPP structure with subwavelength corrugated grooves is etched on the top layer of the SW-HMSIW, which enables flexible design control of slow-wave features by changing the depth of the subwavelength corrugated grooves while at the same time minimizing the longitudinal size. Compared to a conventional SIW with the same electrical length, the longitudinal and lateral dimensions are reduced by 80% and 73%, respectively, with the same cutoff frequency. This represents the most significant SIW size reduction reported in the literature to date. A prototype of the proposed SW-HMSIW-SSPP is manufactured and measurement results are found to agree well with the simulations.

The paper is organized as follows: Section II describes the SW-HMSIW and HMSIW-SSPP topologies, as well as the proposed SW-HMSIW-SSPP topology along with its propagation properties; EM simulations and a theoretical derivation describing the SW effect are presented. Section III analyzes the slow-wave effect of the SW-HMSIW-SSPP from the perspective of an equivalent circuit. Section IV discusses taper transitions that are designed and optimized to match the SW-HMSIW-SSPP structure with microstrip feeder lines for the purpose of measurements, and measurement and simulation results are presented and compared to validate the concept. The paper ends with conclusions in Section V.

II. SLOW WAVE EFFECT ENHANCEMENT

A. SW-HMSIW AND HMSIW-SSPP TOPOLOGIES

Fig. 1 schematically depicts the SW-HMSIW used in our design. The full structure consists of two substrate layers (indicated as Top sub and Bottom sub) and three metal layers (Top metal, Mid metal, and Bottom metal). The thicknesses of the top and bottom substrates are $h_1 = 0.23$ mm and $h_2 = 0.76$ mm, respectively, and the width of the SW-HMSIW, W_s, is set to be 6.7 mm. Lateral via-holes on one side connect the top and the bottom metal layers, acting as a perfect electrical wall in the same manner as in an HMSIW [13]. The lateral width of an HMSIW is decreased by 50% compared with a conventional SIW [15], and the SW-HMSIW can be similarly reduced in size. Considering process capacity and to meet waveguide structure design standards, the period p_1 and the diameter d_1 of the lateral via-holes are chosen to be 1.0 and 0.5 mm. The six rows of internal metallized blind vias-holes connected to the bottom metal have diameters d_2 and separation distance p_2, the latter being the key parameter for the slow-wave effect and which we will analyze and discuss in a separate section below. All blind via-holes are covered with copper lands with diameters d_3. The metallized blind via-holes and lateral via-holes are periodically distributed along the longitudinal direction with the period p_1.

The purpose of loading arrays of metallized blind via-holes inside the HMSIW is to concentrate the electric field in the top substrate layer and to increase the capacitance effect. An increased effective permittivity leads to a reduction of the cutoff frequency and the phase velocity, generating the
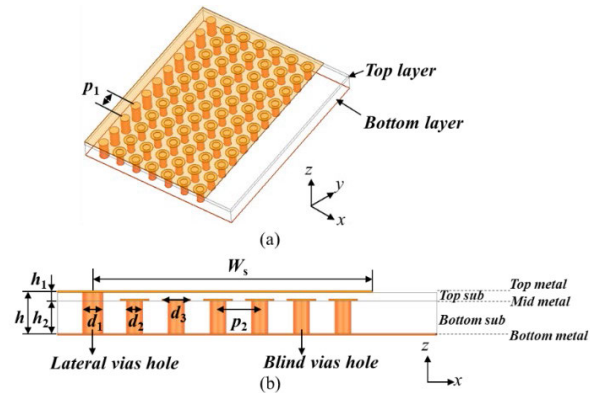

FIGURE 1. Schematic view of the SW-HMSIW [16]. (a) 3-D view. (b) Lateral cross section of the SW-HMSIW.
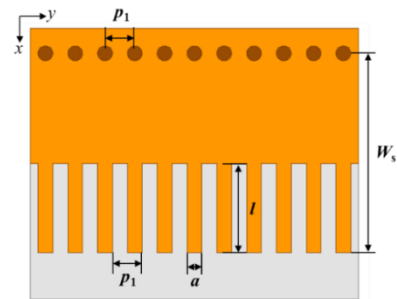

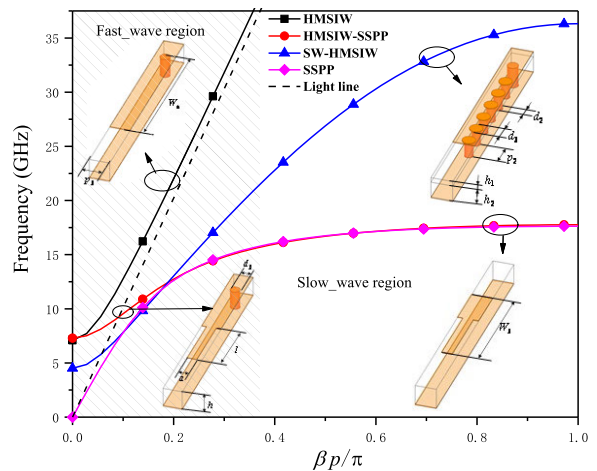**FIGURE 2.** Configurations of HMSIW-SSPP [27].

FIGURE 3. Comparison of dispersion diagrams of HMSIW, SW-HMSIW, HMSIW-SSPP, and SSPP structures.

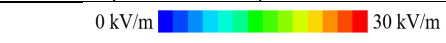slow-wave effect. The design rules for the SW-HMSIW are similar to those of an SW-SIW [15]:
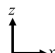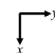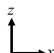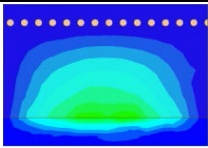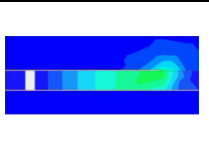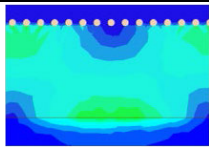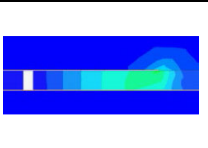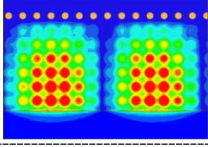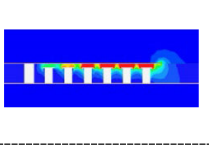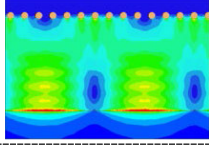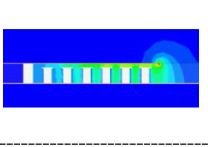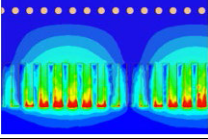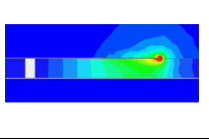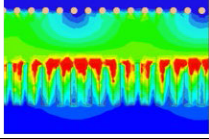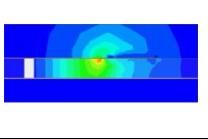
$$\varepsilon_{r\_eff} = \varepsilon_{r1} \cdot \frac{h}{h_1} = \varepsilon_{r1} \cdot (1 + \frac{h_2}{h_1}) \qquad (1)$$

$$f_{c\_SW\text{-}HMSIW} = \frac{c_0}{4 \cdot W_S \cdot \sqrt{\varepsilon_{r\_eff}}} \qquad (2)$$

where ε_{r1} is the relative dielectric constant of the top substrate.

To explore the achievable longitudinal size reduction we consider, the planar SSPP structure shown in Fig.2 is analyzed. The structure of the SSPP, which have periodic

TABLE 1. Electric and magnetic field distributions in HMSIW, SW-HMSIW, and HMSIW-SSPP at 10 GHz.

		E-field Distribution		H-field Distribution	
		Top view	Cross-sectional view	Top view	Cross-sectional view
		0 kV/m ▬▬▬ 30 kV/m		0 A/m ▬▬▬ 80 A/m	
1	HMSIW				
2	SW-HMSIW				
3	HMSIW-SSPP				
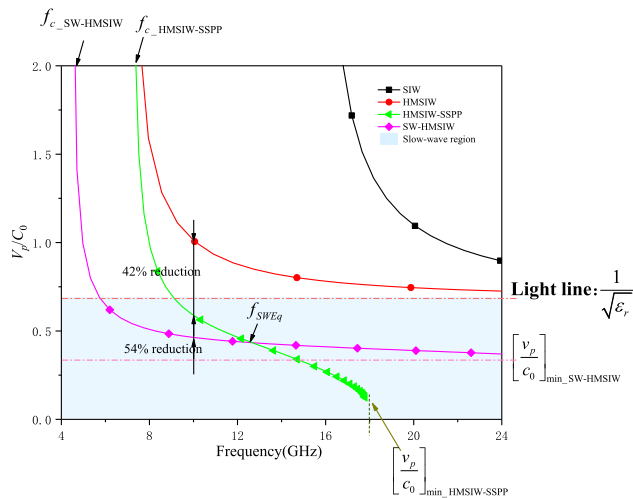
FIGURE 4. Simulated normalized phase velocity versus frequency for the SIW, HMSIW, HMSIW-SSPP, and SW-HMSIW having the same lateral widths.

subwavelength corrugation, is etched on an HMSIW structure fabricated on a single-layered substrate with thickness 0.99 mm. The width is W_s, and the period, width, and depth of the SSPP subwavelength corrugated grooves are p_1, a, and l, respectively. The dispersion relation of this idealized SSPP can be expressed as [29]:

$$\beta = k_0 \sqrt{1 + \frac{a^2}{p_1^2} \tan^2(k_0 \cdot l)} \qquad (3)$$

where β is the propagation constant and $k_0 = \omega/c$.

Although a planar SSPP is different from a true ideal SSPP [32], the planar periodic corrugation has similar characteristics and is able to support and propagate an slow-wave mode.

We compare the slow-wave effect in a range of waveguide transmission line structures by analyzing their dispersion characteristics using the eigenmode analysis tool Ansys HFSS. Analyzed structures are an HMSIW, an SW-HMSIW, an HMSIW-SSPP, and a SSPP, all having identical periodic unit cell parameters (see Fig. 3). Arranging multiple unit cells in succession along the y-axis creates a full transmission line structure akin to that shown in Fig. 2. The model assumes substrates with relative dielectric constant $\varepsilon_r = 2.2$ and dielectric loss tangent $\tan \delta = 0.0009$. The simulated dispersion diagrams are depicted in Fig. 3. We find the dispersion curve of the HMSIW on the left side of the light line indicating that it supports fast waves. The dispersion curve of the SSPP structure is on the right side of the light line, indicating that it supports a pure slow-wave fundamental mode. We note that the dispersion curve of the HMSIW-SSPP structure starts at the lowest cutoff frequency, which is identified as the lowest cutoff frequency of the HMSIW, after which it intersects the light line, deviates from the light line approaching the dispersion curve of the SSPP, and finally reaches the upper cutoff frequency in keeping with (3). We can therefore conclude that the slow-wave effect can be obtained by etching a subwavelength corrugation on the HMSIW structure.

Analogously, the dispersion curve of the SW-HMSIW structure starts at the lowest cutoff frequency, indicating that it supports fast waves in this frequency range. After the dispersion curve intersects the light line, it gradually moves away from the light line as the frequency increases until reaching an upper cutoff frequency, i.e., it supports slow waves in the frequency range from the light line intersection point to the intersection point of the upper cutoff frequency. The lower cutoff frequency of the SW-HMSIW is lower than that of the HMSIW-SSPP, and thus a larger lateral size

reduction can be achieved with the SW-HMSIW. The larger the deviation of the dispersion curve from the light line with increasing frequency, the more pronounced the attenuation of the phase velocity. As can be seen in Fig. 3, the dispersion curve of the HMSIW-SSPP deviates from the light line more sharply than that of the SW-HMSIW, indicating that the phase velocity attenuation of the HMSIW-SSPP is more evident with increasing of frequency.

To gain a better understanding of the slow-wave features of the structures, we compare the electric (E-) field and magnetic (H-) field distributions of the SW-HMSIW and HMSIW-SSPP with those in the conventional HMSIW.

Rows 1 and 2 of TABLE 1 show the magnitude distributions of the E-field at 10 GHz inside the HMSIW and the SW-HMSIW, both having the same lateral and longitudinal dimensions. Looking at the cross-sectional view of the E-field, we can see that the E-field distribution of the HMSIW is uniform, while the E-field distribution of the SW-HMSIW is non-uniform and concentrated between the blind via-holes and the upper ground plane, which is due to the loading of the metallized blind via-holes. From the cross-sectional views of the H-field, we find that the H-field distributions of the HMSIW and SW-HMSIW are both uniform along the z-axis. The effective spatial separation of electric and magnetic fields is a characteristic phenomenon of SW transmission lines. We can observe that the wavelength of the SW-HMSIW structure is significantly reduced in comparison with that of the HMSIW. A reduction of more than 50% can be achieved in the longitudinal direction at 10 GHz.

Comparing the simulated E-field and H-field magnitude distributions of the HMSIW-SSPP structure, shown in Row 3 of TABLE 1 with those of the HMSIW structure we find that, in the cross-sectional view, the E-fields are uniform and mainly concentrated at the open side with a quasi-magnetic wall. The strongest point of the H-field for the HMSIW-SSPP structure is located at the edge of subwavelength corrugated grooves far from the open side, whereas the HMSIW's H-field is uniform. The HMSIW-SSPP structure also shows the separation of electric and magnetic fields typical for slow-wave transmission lines. By comparing of the wavelengths of the HMSIW-SSPP and the HMSIW, we find that a size reduction of more than 40% as compared to the HMSIW is possible for the HMSIW-SSPP structure.

Thus, we find the SW-HMSIW structure to be preferable to the HMSIW-SSPP structure from the point-of-view of achievable longitudinal size reduction at 10 GHz.

At constant frequency wavelength is proportional to the wave speed and hence the rate of change of the phase velocity is equal to the rate of change of the longitudinal length required to propagate the same amount of wave. To quantitatively analyze the possible longitudinal size reduction, we define a normalized phase velocity as the ratio between the phase velocity (v_p) and the light velocity (c_0), where the phase velocity is

$$v_p = \frac{\omega}{\beta} \qquad (4)$$

Normalized phase velocity of the SW-HMSIW, HMSIW-SSPP, and HMSIW structures having the same lateral dimensions are plotted in Fig. 4, and we find the cutoff frequencies to be 4.5, 7.1, and 15.8 GHz, respectively. Hence, the transverse size of the SW-HMSIW structure is reduced by about 37% compared with that of the HMSIW structure and 71.5% as compared to the SIW with the same lateral width. The phase velocities at 10 GHz of the HMSIW-SSPP and SW-HMSIW structures are reduced by 42% and 54% relative to the HMSIW structure, respectively.

B. COMPARISON OF HMSIW-SSPP WITH SW-HMSIW IN THE SLOW-WAVE FREQUENCY BAND

Here we analyze and compare the slow-wave effect in the SW-HMSIW and HMSIW-SSPP theoretically. Areas shaded in light blue in Fig. 4 represent the slow-wave region below the light line, i.e., the region where the transmission lines only support slow waves. To compare the normalized phase velocities of the SW-HMSIW and HMSIW-SSPP we calculate the cut-off frequency point and the phase velocity minimum.

Considering only the primary mode, TE_{10}, for a single-layer substrate SIW, we can express the following relations:

$$\beta_{10} = \sqrt{\omega^2 \mu_0 \varepsilon_0 \mu_r \varepsilon_r - \left(\frac{\pi}{w_{eff\_SIW}}\right)^2} \qquad (5)$$

$$v_{p\_10} = \frac{\omega}{\beta_{10}} = \frac{\omega}{\sqrt{\omega^2 \mu_0 \varepsilon_0 \mu_r \varepsilon_r - \left(\frac{\pi}{w_{eff\_SIW}}\right)^2}} \qquad (6)$$

$$f_{c\_10} = \frac{c_0}{2 w_{eff\_SIW} \sqrt{\mu_r \varepsilon_r}} \qquad (7)$$

$$w_{eff\_SIW} = 2 * w_{eff\_HMSIW}$$
$$= (2W_s) - 1.08 \times \frac{d_1^2}{p_1} + 0.1 \times \frac{d_1^2}{(2W_s)} \qquad (8)$$

The light line, i.e., the dividing line between fast and slow waves, is expressed in the v_p-f diagram (see Fig. 4) as:

$$\frac{v_{p\_10}}{c_0} = \frac{1}{\sqrt{\varepsilon_r}} \qquad (9)$$

The effective relative permittivity of the HMSIW loaded with metallized blind via-holes, is defined in the literature [15] as:

$$\varepsilon_{r\_eff} = \varepsilon_r \cdot \left(1 + \frac{h_2}{h_1}\right) \qquad (10)$$

Substituting (10) into (6)(7) yields:

$$v_{p\_10} = \frac{\omega}{\sqrt{\omega^2 \mu_0 \varepsilon_0 \mu_r \varepsilon_{r\_eff} - \left(\frac{\pi}{w_{eff\_SIW}}\right)^2}} \qquad (11)$$

$$f_{c\_10} = \frac{c_0}{2 w_{eff\_SIW} \sqrt{\mu_r \varepsilon_{r\_eff}}} \qquad (12)$$

In this case, the minimum value of the dispersion curve for the SW-HMSIW in the slow-wave region can be

approximated to be:

$$\left[\frac{v_{p\_10}}{c_0}\right]_{\min} = \frac{1}{\sqrt{\varepsilon_{r\_eff}\,\mu_r}} \qquad (13)$$

From the literature [27] it is furthermore known that the cut-off frequency of the HMSIW with SSPP is equal to the cut-off frequency of the HMSIW. The principle of SSPP can be understood in terms of the dispersion relation of an ideal SSPP, for which the phase velocity is:

$$v_{p\_SSPP} = \frac{c_0}{\sqrt{1 + \frac{a^2}{p^2}\tan^2\left(\frac{\omega l}{c_0}\right)}} \qquad (14)$$

Clearly, $\frac{v_{p\_SSPP}}{c_0}$ is minimized for $\frac{\omega l}{c_0} \rightarrow \frac{\pi}{2} + k\pi(k = 0, 1, 2\cdots)$. If $k = 0$, then ω has physical significance, being:

$$\omega = \frac{\pi c_0}{2 \cdot l} \qquad (15)$$

Therefore, the minimum value of the HMSIW-SSPP dispersion curve in the slow wave region will approach 0 but not equal to 0 due to the presence of substrate loss.

From the above derivation it follows that the normalized phase velocity curves of the two loaded metallized blind via-holes (SW-HMSIW and HMSIW) and the loaded SSPP display monotonic decrease and that the following holds true:

$$f_{c\_SW\text{-}HMSIW} = \frac{c_0}{2w_{eff\_SIW}\sqrt{\mu_r \varepsilon_{r\_eff}}}$$
$$< f_{c\_HMSIW} = \frac{c_0}{2w_{eff\_SIW}\sqrt{\mu_r \varepsilon_r}}$$
$$= f_{c\_HMSIW\text{-}SSPP} \qquad (16)$$

and

$$\left[\frac{v_p}{c_0}\right]_{\min\_SW\text{-}HMSIW} > \left[\frac{v_p}{c_0}\right]_{\min\_HMSIW\text{-}SSPP} \qquad (17)$$

Therefore, there must exist a frequency point f_{SWEq} such that $\left[\frac{v_{p\_SW\text{-}HMSIW}}{c_0}\right] = \left[\frac{v_{p\_HMSIW\text{-}SSPP}}{c_0}\right]$.

We can thus summarize the circuit design advantages and disadvantages of transverse capacitive loading and longitudinal inductive loading:

1. Metallized blind via-hole arrays have a large effect on the cut-off frequency. For frequencies below the frequency point f_{SWEq}, the effect of metallized blind via-hole arrays on the phase velocity reduction is larger compared that for SSPP loading. The equivalent capacitive slow-wave effect requires larger size to accommodate a large periodic array of blind via-holes, and as the slow-wave effect is larger than for SSPP at low frequencies, metallized blind via-hole array loading is suitable for low frequency microwave circuits.

2. For frequencies above the frequency point f_{SWEq}, the phase velocity reduction is larger for SSPP compared to metallized blind via-hole array loading. SSPP has a simple structure, a larger tolerance to fabrication defects, and a larger slow-wave effect at high frequencies, which makes it suitable for high frequency microwave circuits.
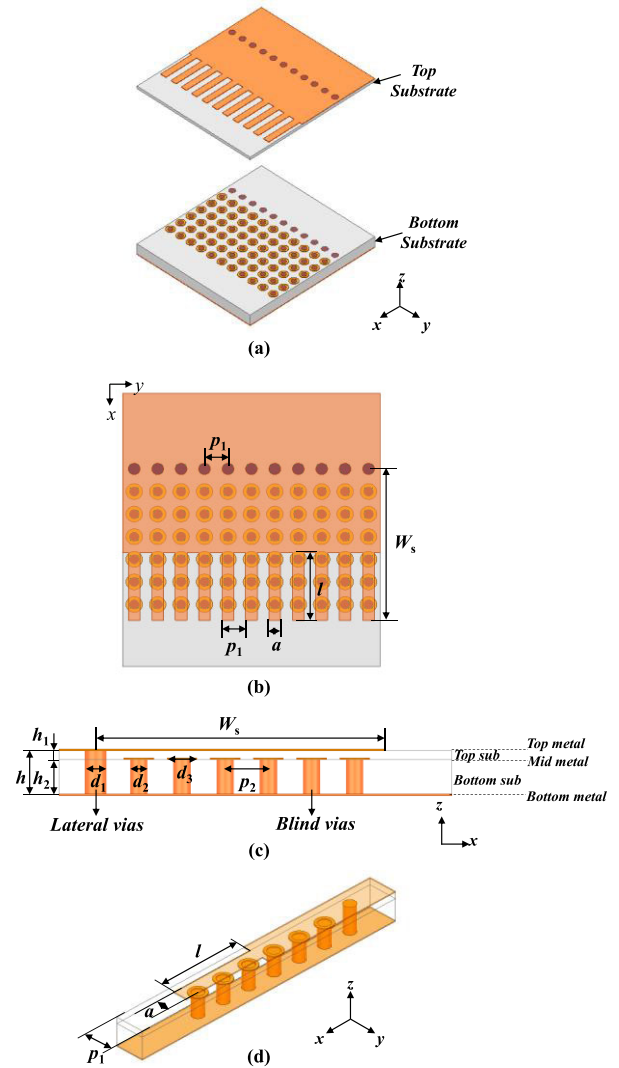
FIGURE 5. Schematic view of the SW-HMSIW-SSPP structure. (a) Expanded 3-D view. (b) Top view. (c) Transversal cross section. (d) One unit cell.

We can thus conclude that the combination of the two types of loading could significantly improve the slow wave effect, which we will analyze in further detail in Section III.

C. SW-HMSIW-SSPP TOPOLOGY AND PROPAGATION PROPERTIES

The SW-HMSIW-SSPP structure proposed in this paper, depicted in Fig. 5, further improves SIW miniaturization by combining metallized blind via-hole arrays and an SSPP structure. The SW-HMSIW-SSPP unit cell consists of an SW-HMSIW with six blind via-holes at the bottom substrate and an SSPP structure etched on the top metal layer of the SW-HMSIW structure. Note that the subwavelength groove is located between the two rows of via-holes along the x direction. The full periodic structure is based on two SYTECH GF220 substrates, which have a relative dielectric constant $\varepsilon_r = 2.2$ and dielectric loss tangent $\tan \delta = 0.0009$. Structural

parameters are consistent with the SW-HMSIW and HMSIW-SSPP structures discussed above.

FIGURE 6. Dispersion diagrams comparison of the HMSIW, proposed SW-HMSIW-SSPP structure, and blind via-holes SSPP.
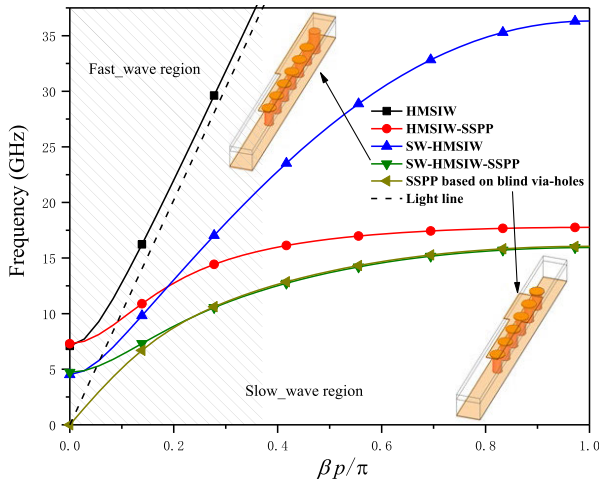
To gain an intuitive understanding of the slow-wave effect in the SW-HMSIW-SSPP structure, consider the simulated dispersion characteristics shown in Fig. 6. The dispersion curve of the SW-HMSIW-SSPP structure starts from the cut-off frequency of the SW-HMSIW, intersects the light line, and converges to that of the blind via-hole SSPP as the frequency increases until an upper cutoff frequency. This implies that the SW-HMSIW-SSPP structure propagates a fast-wave mode at low frequencies while it propagates a slow-wave mode at high frequencies. Furthermore, the dispersion curve of the SW-HMSIW-SSPP is down-shifted compared with the HMSIW-SSPP, which is due to the fact that etching an SSPP on an SW-HMSIW is equivalent to improving the relative dielectric constant of the whole substrate.

The magnitudes of the E- and H-fields of the SW-HMSIW-SSPP structure are shown in Fig. 7. We can observe that the E-field is concentrated close to the open side of the top substrate layer, which indicates an enhancement of the equivalent shunt capacitance of the transmission line that increases the effective permittivity. Furthermore, the H-field is uniform around the metallized vias and the strongest point is at the edge of the subwavelength corrugated grooves far from the open side. This enhances the series inductance, which increases the effective permeability. The effective separation between the electric and the magnetic fields in space is, as mentioned, a typical slow-wave phenomenon. We furthermore find that the longitudinal dimension of the SW-HMSIW-SSPP is reduced by more than 70% as compared to the HMSIW of same electric length.

Fig. 8 shows that the cutoff frequency of the SW-HMSIW-SSPP and the equivalent HMSIW are 4.5 and 7.1 GHz, respectively. Therefore, the lateral dimension of the SW-HMSIW-SSPP is decreased by 37% relative to the HMSIW. The normalized phase velocity of the SW-HMSIW-SSPP is reduced by 74% compared to the HMSIW, as well as reduced by 42% and 54% relative the HMSIW-SSPP
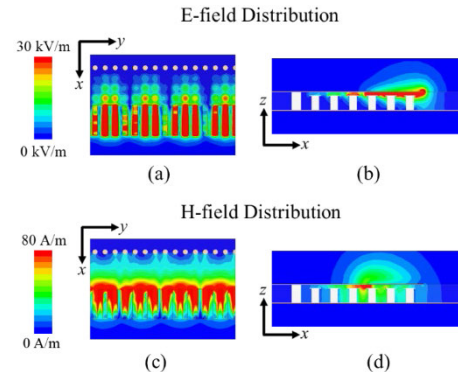

FIGURE 7. Electric and magnetic field distributions in the proposed SW-HMSIW-SSPP at 10 GHz. (a) E-field top view, (b) E-field cross-sectional view, (c) H-field top view, and (d) H-field cross-sectional view.
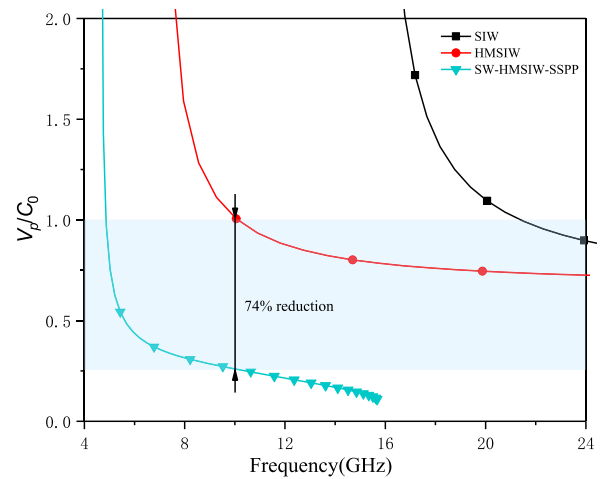

FIGURE 8. Simulated normalized phase velocity versus frequency for the SIW, HMSIW, and the proposed SW-HMSIW-SSPP structures with the same lateral width.

and the SW-HMSIW structures (see Fig. 4), respectively. Thus, the longitudinal length is reduced by 74% compared with the HMSIW. In summary, the above analysis shows that the SW-HMSIW-SSPP structure displays an excellent slow-wave feature based on periodic blind via-holes and the subwavelength corrugation.

To analyze the relationship between the changes in geometry and the slow-wave effect, the dispersion features for different geometrical parameters are shown in Fig. 9. Fig. 9(a) shows the influence of the width of the SSPP structure on the dispersion, and we note that the propagation constant β is not strongly dependent on finger width a. An increase of the finger length l of the SSPP structure yields an increased upper cutoff frequency, as is seen in Fig. 9(b). Fig. 9(c) shows that the lower cutoff frequency increases with increasing structure width W_s, this since the cutoff frequency is inherently inversely proportional to the HMSIW width. As such, finger length l and structure width W_s of the SSPP structure are the most influential parameters for dispersion curve tailoring.

To explore the effect of the internal metallized via-holes on the achievable HMSIW size reduction, the cutoff frequency and normalized phase velocity versus via-diameter are plotted
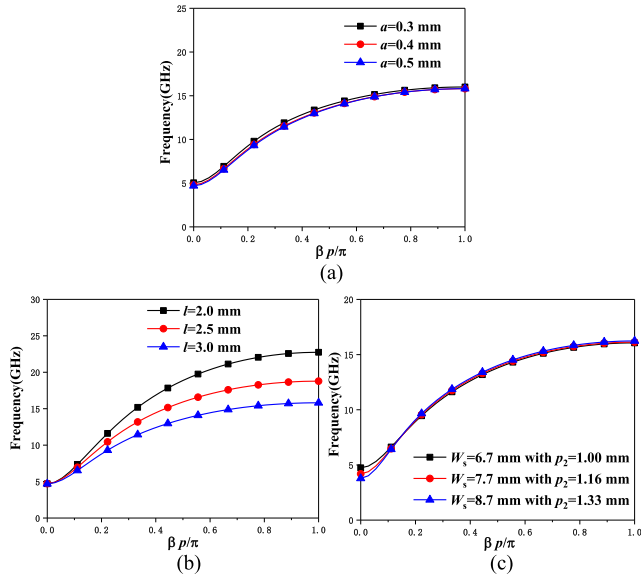
FIGURE 9. Simulated dispersion diagrams of the proposed SW-HMSIW-SSPP structure with different (a) finger width a and (b) finger length l of the SSPP structure; and (c) structure width of SW-HMSIW-SSPP.
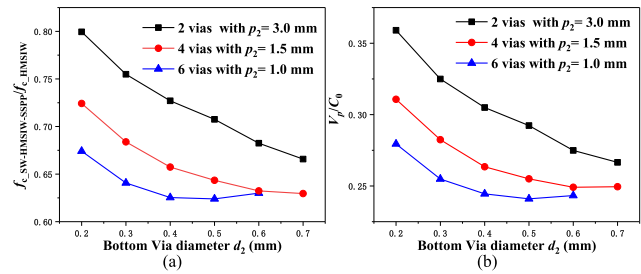

FIGURE 10. (a) Normalized cutoff frequency and (b) normalized phase velocity at 10 GHz versus bottom via diameter.

in Fig. 10. Both the cutoff frequency and the normalized phase velocity decreases with bottom via diameter d_2 and number of via-holes n for the two-via-rows and four-via-rows cases. However, in the six-via-rows case the cutoff frequency and normalized phase velocity do not decrease but rather increases when the via-diameter increases beyond 0.5 mm. This phenomenon can be explained by the H-field behavior: when the distance p_2 between the blind via-holes is short for large blind via-hole diameters, the H-field is susceptible to interference and hence the H-field will concentrate on the top substrate layer rather than be uniformly distributed in the top and bottom substrates flowing around the blind via-holes. Thus, magnetic flux decreases and capacitance no longer increases. For this reason, the six-via-rows case with blind via-hole separation distance $p_2 = 1.0$ mm and blind via-holes diameter $d_2 = 0.5$ mm is considered the design optimum for miniaturization.

III. EQUIVALENT CIRCUIT MODEL OF THE PROPOSED SW-HMSIW-SSPP

In order to do a circuit analysis of the slow-wave effect in the SW-HMSIW-SSPP, we use the equivalent circuit model of a periodic unit shown in Fig. 11. The surface current path of

the top layer of the SSPP can be equated to an inductor, and the equivalent inductance values L_x and L_y can be calculated from the static electromagnetic field [33]:

$$L_x = \frac{\mu_0 l}{2\pi}\left(\ln\frac{2l}{a+t} + \frac{1}{2}\right) \tag{18}$$

$$L_y = \frac{\mu_0(W_s - l)}{2\pi}\left(\ln\frac{2(W_s - l)}{p_1 + t} + \frac{1}{2}\right) \tag{19}$$

where a, and l are the width and depth of the SSPP subwavelength corrugated grooves, and p_1 and t are the period and metal layer thickness of the SSPP structure. With an increasing finger width a, the inductance L_x will decrease, and with increasing finger length l, the inductances L_x and L_y will increase and decrease, respectively. Because the thickness t of the metal layer is much smaller than the finger width a and finger length l, the effect of the metal layer thickness t on the equivalent inductance is negligible. Therefore, the equivalent inductances L_x, L_y can be controlled by the finger length l and finger width a of the SSPP structure.
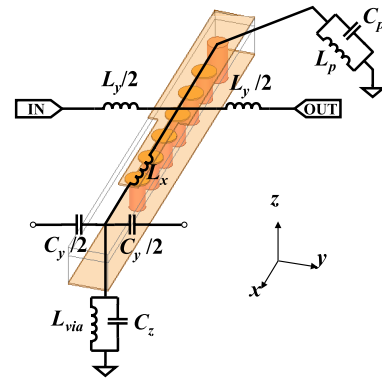

FIGURE 11. Equivalent-circuit model based on SW-HMSIW-SSPP periodic unit.

There are two types of equivalent capacitances in the proposed model. One, C_y, exists between the two SSPP finger plates and it can be calculated using EM wave simulation software. In simple terms, the equivalent capacitance C_y increases as the area of the SSPP finger plate increases and the distance between the two plates decreases. The second equivalent capacitance, C_z, exists between the SSPP finger plate and ground. Compared to the equivalent capacitance C_z, the capacitance C_y is relatively small and negligible [34].

Similarly, the capacitance C_z can be calculated by EM simulation software. The equivalent capacitance, C_z, can be roughly modeled using the capacitance calculation equation for a flat plate capacitor:

$$C = \frac{\varepsilon_r \varepsilon_0 A}{d} \tag{20}$$

where A denotes the area of the flat plate, and d the distance between the plates. From (20) it is easy to see that the smaller the area of the SSPP plate, the smaller the capacitance C_z. As the height of the metallized blind via-holes increases, i.e., the distance to the upper metal layer becomes smaller, the capacitance C_z increases, which in turn increases the overall effective relative permittivity.

For the loaded metallized blind via-holes, an inductance L_{via} will inevitably be introduced, which can be expressed as:

$$L_{via} = \frac{\mu_0}{2\pi} \cdot 4 \left| \ln\left(\frac{4h_2}{d_2}\right) - 1 \right| \cdot h_2 \tag{21}$$

We can see that the inductance of a metallized blind via-hole increases with decreasing diameter d_2 [35], leading to an increase in the equivalent inductance and effective permeability of the SW-HMSIW-SSPP. The metallized via-holes connecting the upper and lower metal layers can furthermore be described by an equivalent parallel circuit of parasitic inductance L_p and parasitic capacitance C_p, which can be calculated using [28]:

$$L_p = 5.08h[\ln(\frac{4h}{d_1}) + 1] \tag{22}$$

$$C_p = 1.41\varepsilon_r h \tag{23}$$

According to the above analysis, the loaded metallized blind via-holes introduce an equivalent capacitance C_z, which affects the overall equivalent permittivity; the loaded planar SSPP introduces equivalent inductances L_x and L_y, which, together with equivalent inductance L_{vias} introduced by the metallized blind via-holes, affect the overall equivalent permeability.

For a miniaturized slow-wave structure, the dissipation of power during energy transmission needs to be considered. The primary cause of power dissipation in this structure can predominantly be attributed to waveguide losses. The waveguide loss comprises, e.g., conductor loss, dielectric loss, radiation loss. The total loss resulting from the various loss mechanisms in the waveguide can be quantified by the attenuation constant, α, of the waveguide [36]. Fig. 12 plots the attenuation constants for unit cells of SW-HMSIW, HMSIW-SSPP and SW-HMSIW-SSPP obtained by simulations (simulation substrate parameters: $\varepsilon_r = 2.2$, $\mu_r = 1$) and we found that at 10 GHz these are 0.007 dB/mm, 0.006 dB/mm and 0.015 dB/mm, respectively, all being within reasonable limits. The reason that the unit cell of SW-HMSIW-SSPP has largest attenuation constant in is that the simultaneous use of the SSPP structure and metallized blind via-holes structure results in a larger electric field concentration between these two structures (see Fig. 7), leading to increased losses.

Although the attenuation constant of the SW-HMSIW-SSPP rapidly increases at frequencies above 15 GHz, it is sufficiently low for today's 5G requirements in the effective operating bandwidth of the structure 4.5 - 12 GHz. Furthermore, the design as presented in this paper is based on a center frequency of 10 GHz, however it can be made to work effectively at higher frequencies with global optimization of the whole structure. In order to quantitatively estimate the equivalent permittivity and permeability, we use the non-periodic loading unit electromagnetic parameter extraction method [37], [38]. TABLE 2 summarizes the normalized phase velocity, slow-wave region frequency band,
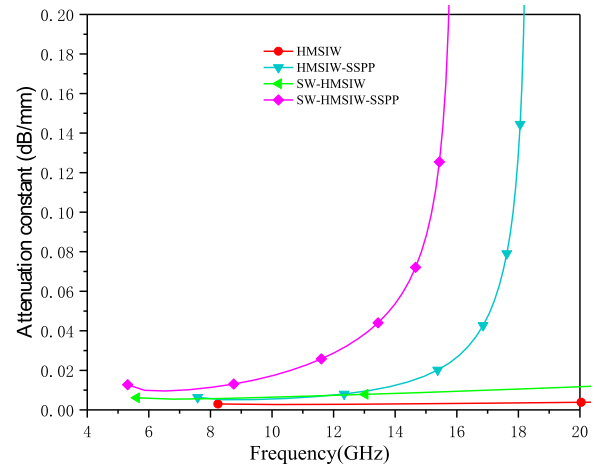

FIGURE 12. Simulated attenuation constants of HMSIW, HMSIW-SSPP, SW-HMSIW and SW-HMSIW-SSPP unit cells.

TABLE 2. Comparison of important performance parameters of SW-HMSIW, HMSIW-SSPP and SW-HMSIW-SSPP at 10 GHz.

	SW-HMSIW	HMSIW-SSPP	SW-HMSIW-SSPP
v_p/c_0	0.46	0.59	0.26
Slow-wave region frequency band (GHz)	(5.8-36)	(9.2-17.8)	(5.1-15.7)
α_u (dB/mm)	0.007	0.006	0.015
f_c (GHz)	4.5	7.1	4.5
ε_r	9	2.2	9
μ_r	0.75	1.28	1.15

attenuation constant and cut-off frequency, as well as the equivalent permittivity and permeability for the SW-HMSIW, HMSIW-SSPP, and SW-HMSIW-SSPP structures.

The equivalent dielectric constants of pure HMSIW and HMSIW-SSPP structure are nearly identical, as the cutoff frequencies of these two structures are close to identical (see Fig. 4). Thus, the equivalent permittivity constant of HMSIW can also be considered as 2.2. The equivalent permittivity is increased by 309% when the HMSIW is transversely loaded with metalized blind via-holes only. However, the equivalent permeability decreases by about 25%, implying a weakening of the equivalent series inductance of the SW-HMSIW, which is a phenomenon neglected in the literature [15]. When the HMSIW is only loaded by SSPP, i.e., longitudinal loading, there is no change in the equivalent permittivity and the equivalent permeability is increased by 28%. Combining longitudinal and transverse loading the equivalent permittivity is increased by 309% and the equivalent permeability by 15%, demonstrating that the SW-HMSIW-SSPP can simultaneously increase the equivalent permittivity and permeability of the substrate. I.e., significant miniaturization of the SW-HMSIW-SSPP is possible.

IV. SIMULATION AND MEASUREMENT RESULTS

A. TRANSMISSION ANALYSIS

The structure of the proposed SW-HMSIW-SSPP including a tapering transition structure is depicted in Fig. 13. It consists of two substrates, both with $\varepsilon_r = 2.2$ and $\tan\delta = 0.0009$, stacked together by a Rogers 4450F prepreg with 0.102 mm thickness, as shown in Fig. 13(b). The top substrate is Taconic TLY-5 with 0.13 mm thickness and the bottom substrate is SYTECH GF220 with 0.76 mm thickness. The tapering transition structure that connects the SW-HMSIW-SSPP structure to a microstrip line (ML) is designed for impedance matching and measurement convenience. As shown in Fig. 13(a), the transition consists of two parts: part (1), being a conventional 50 Ω microstrip loaded with one column of blind via-holes to the bottom substrate to transition between the ML and SW-HMSIW, and part (2), in which the finger length gradually changes from $0.1*l$ to l to transition between the SW-HMSIW and SW-HMSIW-SSPP. Fig. 14 compares the E-field distributions of the entire proposed SW-HMSIW-SSPP structure and an equivalent HMSIW. We note that, in the SW-HMSIW-SSPP the E-field is strongly concentrated in the finger shaped surfaces of the SSPP structure. The geometry parameters of the proposed structure following optimization using Ansys HFSS are listed in TABLE 3.

The SW-HMSIW-SSPP structure can be considered as a two-port transmission network, and obtain the transmission characteristics by calculating the S-parameters through simulations. Based on the definition of a two-port transmission network, $|S_{11}|^2$, can be used to estimate the percentage of reflected power at the input port due to the impedance mismatch relative to the input power, and $|S_{21}|^2$ can be used to evaluate the ratio of output power to input power [39]. Therefore, the power reflected back from the input port, P_{inr}, and the output power, P_{out}, can be calculated as:

$$P_{inr} = P_{in} \times |S_{11}|^2 \qquad (24)$$

$$P_{out} = P_{in} \times |S_{21}|^2 \qquad (25)$$

In the simulation, the excitation port is set with an input power (P_{in}) of 1W (or 30 dBm). Note that, there is no need to distinguish between input and output ports due to the symmetry of the proposed SW-HMSIW-SSPP structure. As shown in Fig. 15, the proposed structure exhibits minimal reflected power within the frequency range of 4.8 GHz to 11.5 GHz, and it achieves a maximum output power exceeding 0.8 W. Due to the increase in the attenuation constant with frequency (see Fig. 12), the output power of the SW-HMSIW-SSPP structure experiences a rapid decline when operating above 12 GHz.

B. SIMULATION RESULTS

To illustrate the potential for lateral size reduction, the transmission coefficients (S_{21}) of SIW, HMSIW, SW-HMSIW, and the SW-HMSIW-SSPP structures, all with the same cut-off frequency (f_c), are simulated, the results of which are shown in Fig. 16. For cutoff frequency $f_c = 4.5$ GHz
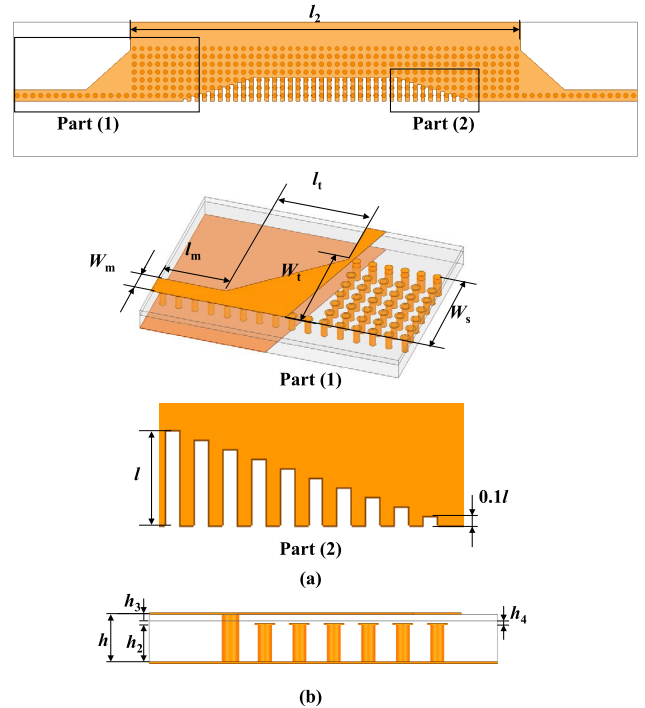

FIGURE 13. (a) Configurations of the SW-HMSIW-SSPP and the tapering transition structure. (b) Transversal cross section of the SW-HMSIW-SSPP.
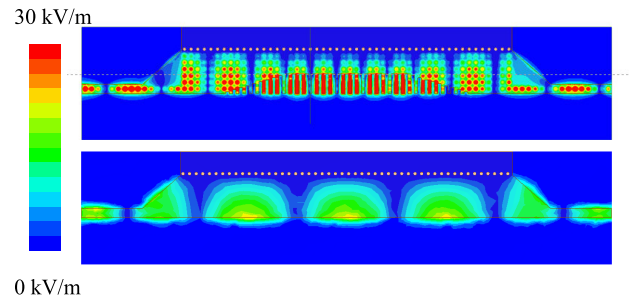

FIGURE 14. E-field distributions of the proposed SW-HMSIW-SSPP structure and an equivalent HMSIW structure.

of the proposed SW-HMSIW-SSPP structure, the widths of the equivalent SIW, the HMSIW, and the SW-HMSIW are 22.5 mm, 11.25 mm, and 6.7 mm. I.e., the width of the proposed SW-HMSIW-SSPP structure is reduced by about 40% and 70% as compared with the HMSIW and SIW structures, respectively.

The simulated SW-HMSIW-SSPP scattering parameters are plotted in Fig. 18. The cutoff frequency is 4.5 GHz and the reflection is below −10 dB in the range 5.2 to 12 GHz. As can be seen in Fig. 20, the simulated normalized phase velocity of the optimized SW-HMSIW-SSPP is reduced by about 74% compared with the HMSIW with the same lateral dimension, i.e., same as obtained for the periodic unit based on normalized phase velocity (Fig. 4). The simulated attenuation constant is 0.016 dB/mm at 10 GHz (Fig. 21).

C. MEASUREMENT RESULTS

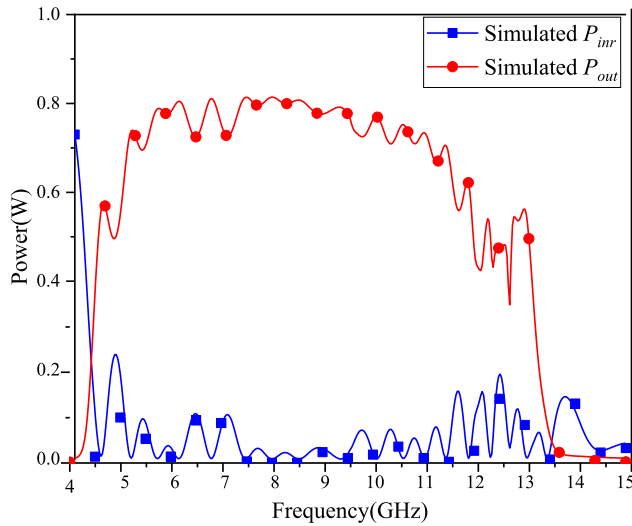A fabricated PCB SW-HMSIW-SSPP structure with a total size of 80 mm × 30 mm including the taper transition is

FIGURE 15. Simulation results of reflected power P_{inr} and output power P_{out} for the proposed SW-HMSIW-SSPP structure.

TABLE 3. Geometrical parameters of SW-HMSIW-SSPP (UNITS: MILLIMETERS).

Variable	p_1	W_s	h_1	h_2	h	d_1	d_2	d_3	p_2	l
Value	1.0	6.7	0.23	0.76	0.99	0.5	0.4	0.6	1.0	3.0
Variable	a	W_1	W_m	l_m	l_t	W_t	l_2	h_3	h_4	
Value	0.5	5.0	1.4	9.3	5.7	6.7	50	0.13	0.102	

shown in Fig. 17. S-parameters were measured using an Agilent N5247A network analyzer, and results are plotted in Fig. 18 together with the simulation results. The simulation and measurement results agree reasonably well with each other; however, the measured cutoff frequency is 4.2 GHz, i.e., shifted 0.3 GHz compared with the simulation result, which we attribute to fabrication error. To verify this hypothesis, S-parameters for an SW-HMSIW-SSPP having a compression error yielding a 50um thickness reduction are simulated. As can be seen in the results shown in Fig. 19, the cutoff frequency of the SW-HMSIW-SSPP with the compression error is lower than in the error-free case, indicating that a compression error is the main reason for the lower measured cut-off frequency. As the thickness of the prepreg will inevitably be somewhat reduced during the process of pressing the multilayer together, the measured impedance bandwidth of 4.8 - 11.5 GHz will consequently be slightly narrower than the simulation result (5.2 - 12 GHz).

Comparing the cutoff frequency of the SW-HMSIW-SSPP with that of an SIW (f_{c_SIW} = 15.8 GHz) designed with the same lateral dimension, a reduction of the lateral width of more than 73% is obtained.

The measured normalized phase curve of the optimized SW-HMSIW-SSPP are consistent simulation results as can be seen in Fig. 20. As the simulation results for the
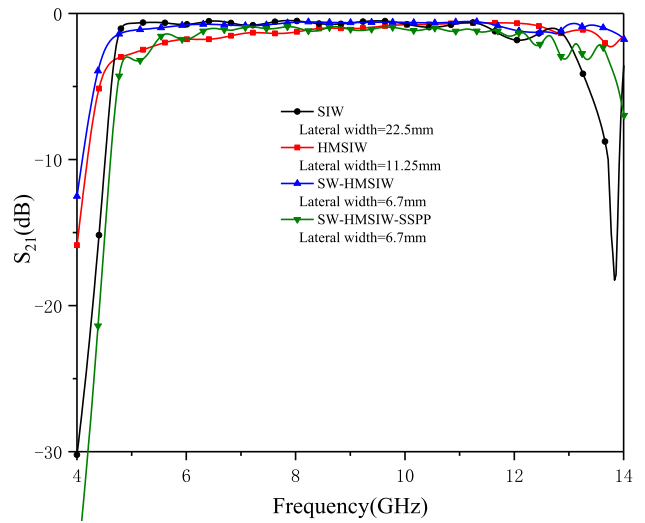

FIGURE 16. Simulation results of transmission coefficient S_{21} of SIW, HMSIW, SW-HMSIW, and the proposed SW-HMSIW-SSPP structures, all having the same cut-off frequency.
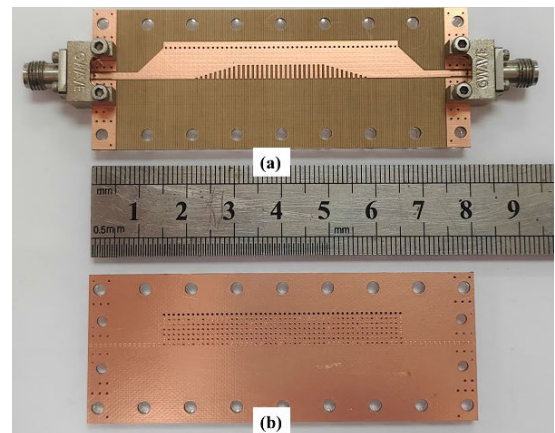

FIGURE 17. Fabricated PCB sample of the SW-HMSIW-SSPP structure. (a) Top view. (b) Bottom view.
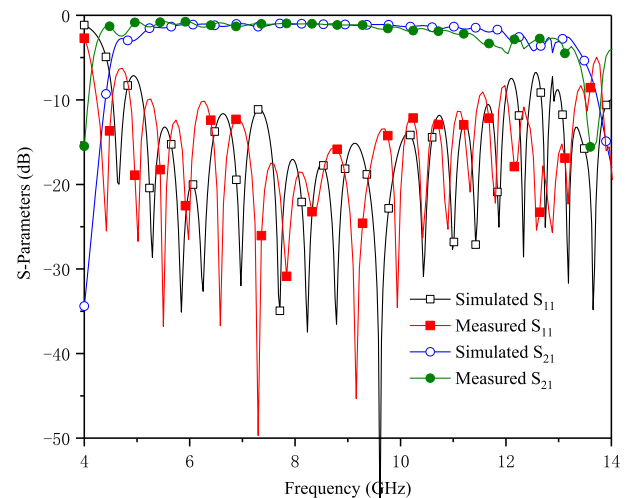

FIGURE 18. Measured and simulated reflection (S_{11}) and transmission coefficients (S_{21}) of the proposed SW-HMSIW-SSPP.

normalized phase curves of the SW-HMSIW-SSPP with compression errors in general agree with measurement results,

TABLE 4. Performance comparison of SIW slow-wave structures proposed in the literature.

Ref. No	Type	Freq. (GHz)	BW (GHz)	Longitudinal Reduction (%)	Lateral Reduction (%)	Attenuation Constant (dB/mm)	No. of Layers	Cross-section thickness (mm)
[15]	SIW with blind via-holes	12	9.3-18	40	40	0.03	2	1.113
[17]	SIW with microstrip polyline	12	4.0-17	40	40	0.02	1	0.5
[18]	SIW with lumped inductor	5.5	3.5-8	35	35	-	1	0.5
[19]	SIW with ring-mushroom	7	-	>40	>40	0.008	1	1.27
[20]	SIW with antipodal blind via-holes	5	5.1-9.6	>50	55	0.018	3	1.118
[21]	SIW with blind via-holes and shorted patch	11	7.1-18.8	73	53	0.02	2	1.016
[27]	HMSIW with SSPP	12	7.2-15.8	>50	50	0.016	1	0.5
[28]	HMSIW with 2.5D SSPP	10	6-14	>50	65	0.035	1	0.508
[29]	RHMSIW with SSPP	10	4.5-14	>50	>70	-	2	0.762
[31]	HMSIPW	3.34 5.16	3.02-3.66 4.66-5.65	>60	19.4	-	1	0.127
	Our Work	10	4.8-11.5	>80	>73	0.02	3	0.992
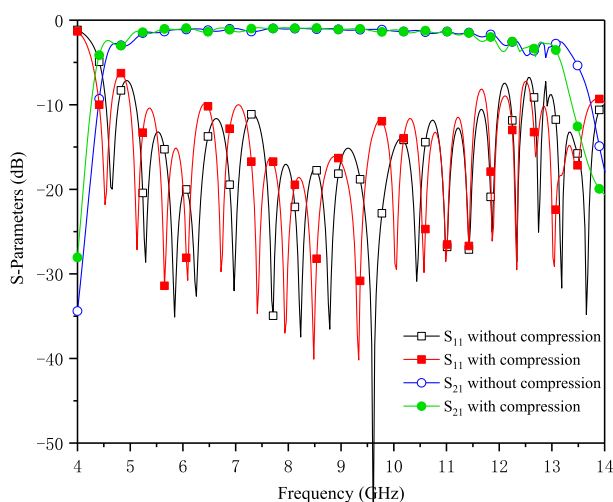
FIGURE 19. Simulated S-parameters of the SW-HMSIW-SSPP with and without the compresses error.

FIGURE 20. Measured and simulated normalized phase velocity of the optimized SW-HMSIW-SSPP and the HMSIW.

we conclude that the differences observed between measured and simulated phase velocities are mainly due to compression discrepancies. The measurement results confirm
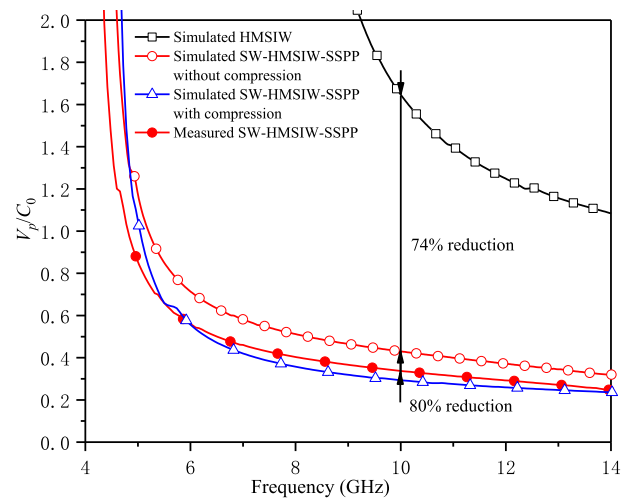
that the SW-HMSIW-SSPP allows for an 80% waveguide electrical length reduction as compared to a conventional HMSIW. The measured attenuation constant of the proposed
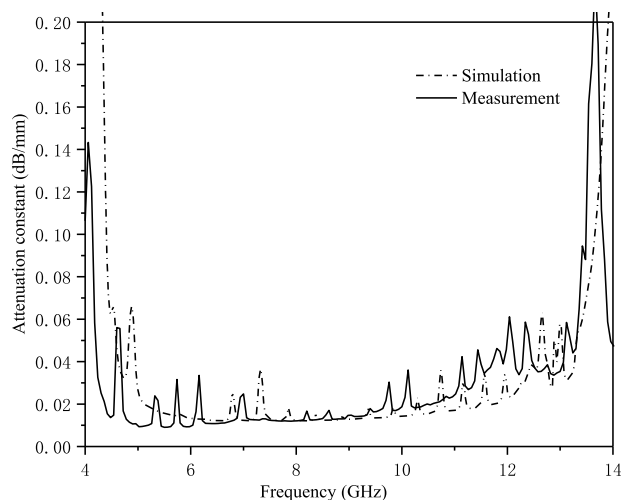
FIGURE 21. Measured and simulated attenuation constants of the proposed SW-HMSIW-SSPP.

SW-HMSIW-SSPP is 0.02 dB/mm at 10 GHz, shown in Fig. 21 together with results from computer simulations of the same.

In TABLE 4 we compare the pertinent parameters and performance between our proposed SW-HMSIW-SSPP and those of previously published approaches for SIW miniaturization. Although the longitudinal size reduction of the design in [24] reached 70%, the aspects of the attenuation constant and insertion loss for RHMSIW with SSPP in [29] are not discussed in sufficient detail to be able to be compared with the SW-HMSIW-SSPP. Compared with the SIW loading blind via-holes and shorted patch [21], the etched SSPP structure of the SW-HMSIW-SSPP allows for simple dispersion curve design through adjustment of the geometric parameters. The work reported in [31] is a diplexer based on a half-mode substrate integrated plasmonic waveguide (HMSIPW) in which the longitudinal size was reduced significantly (over 60%), however the lateral size reduction was very limited. Although the thickness of the proposed SW-HMSIW-SSPP is larger than that in some of the other designs [17], [18], [27], [28], [29], [31] it achieves the largest longitudinal and lateral size reduction reported while having a low attenuation constant.

V. CONCLUSION

In this paper, an SW-HMSIW-SSPP structure based on metallized blind via-hole arrays and a spoof surface plasmon polariton structure is presented, analyzed, and demonstrated with a PCB processed experimental prototype. According to dispersion curve analysis, the proposed structure supports hybrid fast and slow wave modes. The proposed structure displays the typical slow-wave phenomena of effective electric and the magnetic field spatial separation. The simultaneous increase of the effective permeability and permittivity in the SW-HMSIW-SSPP structure allows for superior miniaturization as compared to previously reported SW structures. The results show longitudinal and lateral size reductions of the SW-HMSIW-SSPP of more than 80% and 73%, respectively,

as compared with an equivalent SIW at the same frequency, with maintained low attenuation constant. The proposed structure has potential application uses in miniaturized filters, couplers, and leaky-wave antennas.

REFERENCES

[1] A. Zhao and Z. Ren, "Size reduction of self-isolated MIMO antenna system for 5G mobile phone applications," *IEEE Antennas Wireless Propag. Lett.*, vol. 18, pp. 152–156, 2019, doi: 10.1109/LAWP.2018.2883428. https://doi.org/10.1109/Lawp.2018.2883428.

[2] T. G. Bryant and J. A. Weiss, "Parameters of microstrip transmission lines and of coupled pairs of microstrip lines," *IEEE Trans. Microwave Theory Techn.*, vols. MTT-16, no. 12, pp. 1021–1027, Dec. 1968, doi: 10.1109/TMTT.1968.1126858.

[3] C. P. Wen, "Coplanar waveguide: A surface strip transmission line suitable for nonreciprocal gyromagnetic device applications," *IEEE Trans. Microwave Theory Techn.*, vols. MTT-17, no. 12, pp. 1087–1090, Dec. 1969, doi: 10.1109/TMTT.1969.1127105.

[4] R. J. Beneck, A. Das, G. Mackertich-Sengerdy, R. J. Chaky, Y. Wu, S. Soltani, and D. Werner, "Reconfigurable antennas: A review of recent progress and future prospects for next generation," *Prog. Electromagn. Res.*, vol. 171, pp. 89–121, 2021.

[5] T. Han, B. Dong, Y. Zhang, Y. Wang, Z. Yan, H. Zhou, J. Feng, and Y. Liu, "Research on the radiation properties of tapered slot magnetoelectric antenna," *Prog. Electromagn. Res.*, vol. 177, pp. 75–84, 2023, doi: 10.2528/pier23030802.

[6] X. Li, H. Q. Yang, R. W. Shao, F. Zhai, G. B. Liu, Z. X. Wang, H. F. Gao, G. Fan, J. W. Wu, Q. Cheng, and T.-J. Cui, "Low cost and high performance 5-bit programmable phased array antenna at Ku-band," *Prog. Electromagn. Res.*, vol. 175, pp. 29–43, 2022, doi: 10.2528/pier22052806.

[7] K. Wu, D. Deslandes, and Y. Cassivi, "The substrate integrated circuits—A new concept for high-frequency electronics and optoelectronics," in *Proc. 6th Int. Conf. Telecommun. Modern Satell., Cable Broadcast. Service*, 2003, pp. 3–10.

[8] D. Deslandes and K. Wu, "Accurate modeling, wave mechanisms, and design considerations of a substrate integrated waveguide," *IEEE Trans. Microwave Theory Techn.*, vol. 54, no. 6, pp. 2516–2526, Jun. 2006, doi: 10.1109/TMTT.2006.875807.

[9] Y. Liu, Y. Zhang, C. Meng, H. Liu, B. Liu, and S. He, "A dual-board substrate integrated waveguide for large phase delay application," in *Proc. Photon. Electromagn. Res. Symp.*, Nov. 2021, pp. 180–183.

[10] P. Luo, W. He, Y. Zhang, H. Liu, E. Forsberg, and S. He, "Leaky-wave antenna with wide scanning range based on double-layer substrate integrated waveguide," *IEEE Access*, vol. 8, pp. 199899–199908, 2020.

[11] D.-F. Guan, Q. Zhang, P. You, Z.-B. Yang, Y. Zhou, and S.-W. Yong, "Scanning rate enhancement of leaky-wave antennas using slow-wave substrate integrated waveguide structure," *IEEE Trans. Antennas Propag.*, vol. 66, no. 7, pp. 3747–3751, Jul. 2018.

[12] M. Bozzi, S. A. Winkler, and K. Wu, "Broadband and compact ridge substrate-integrated waveguides," *IET Microwave, Antennas Propag.*, vol. 4, no. 11, p. 1965, Nov. 2010, doi: 10.1049/iet-map.2009.0529.

[13] Q. Lai, C. Fumeaux, W. Hong, and R. Vahldieck, "Characterization of the propagation properties of the half-mode substrate integrated waveguide," *IEEE Trans. Microwave Theory Techn.*, vol. 57, no. 8, pp. 1996–2004, Aug. 2009.

[14] N. Grigoropoulos, B. Sanz-Izquierdo, and P. R. Young, "Substrate integrated folded waveguides (SIFW) and filters," *IEEE Microwave Wireless Compon. Lett.*, vol. 15, no. 12, pp. 829–831, Dec. 2005, doi: 10.1109/LMWC.2005.860027.

[15] A. Niembro-Martín, V. Nasserddine, E. Pistono, H. Issa, A.-L. Franc, T.-P. Vuong, and P. Ferrari, "Slow-wave substrate integrated waveguide," *IEEE Trans. Microwave Theory Techn.*, vol. 62, no. 8, pp. 1625–1633, Aug. 2014.

[16] J. Li, C. Ding, F. Wei, and X. Wei Shi, "Compact UWB BPF with notch band based on SW-HMSIW," *Electron. Lett.*, vol. 51, no. 17, pp. 1338–1339, Aug. 2015, doi: 10.1049/el.2015.0449.

[17] H. Jin, K. Wang, J. Guo, S. Ding, and K. Wu, "Slow-wave effect of substrate integrated waveguide patterned with microstrip polyline," *IEEE Trans. Microwave Theory Techn.*, vol. 64, no. 6, pp. 1717–1726, Jun. 2016.

[18] H. Jin, Y. Zhou, Y. M. Huang, and K. Wu, "Slow-wave propagation properties of substrate integrated waveguide based on anisotropic artificial material," *IEEE Trans. Antennas Propag.*, vol. 65, no. 9, pp. 4676–4683, Sep. 2017.

[19] X. Li, K. Dhwaj, and T. Itoh, "Single-layer slow-wave substrate integrated waveguide with enhanced capacitance," in *IEEE MTT-S Int. Microwave Symp. Dig.*, Jun. 2018, pp. 316–318.

[20] Y. Zhou, H. Jin, Y. M. Huang, D. Xu, S. Ding, P. Wang, M. Bozzi, and L. Perregrini, "Slow-wave effect enhanced substrate integrated waveguide with multi-antipodal blind via-holes and distributed metal strips," *IEEE Microwave Wireless Compon. Lett.*, vol. 30, no. 8, pp. 753–756, Aug. 2020.

[21] Y. Zhang, J.-Y. Deng, D. Sun, J.-Y. Yin, L.-X. Guo, X.-H. Ma, and Y. Hao, "Slow wave substrate-integrated waveguide with miniaturized dimensions and broadened bandwidth," *IEEE Trans. Microwave Theory Techn.*, vol. 69, no. 8, pp. 3675–3683, Aug. 2021, doi: 10.1109/TMTT.2021.3074170.

[22] H. Raether, "Surface plasmons on smooth surfaces," in *Tracts in Modern Physics*. Cham, Switzerland: Springer, 1988, pp. 4–39.

[23] J. B. Pendry, L. Martin-Moreno, and F. J. Garcia-Vidal, "Mimicking surface plasmons with structured surfaces," *Science*, vol. 305, no. 5685, pp. 847–848, Aug. 2004, doi: 10.1126/science.1098999.

[24] F. J. Garcia-Vidal, L. Martín-Moreno, and J. B. Pendry, "Surfaces with holes in them: New plasmonic metamaterials," *J. Opt. A, Pure Appl. Opt.*, vol. 7, no. 2, pp. S97–S101, Feb. 2005, doi: 10.1088/1464-4258/7/2/013.

[25] A. P. Hibbins, B. R. Evans, and J. R. Sambles, "Experimental verification of designer surface plasmons," *Science*, vol. 308, no. 5722, pp. 670–672, Apr. 2005, doi: 10.1126/science.1109043.

[26] L. Liu and Z. Li, "Spoof surface plasmons arising from corrugated metal surface to structural dispersion waveguide," *Prog. Electromagn. Res.*, vol. 173, pp. 93–127, 2022, doi: 10.2528/pier22011301.

[27] D.-F. Guan, P. You, Q. Zhang, Z.-B. Yang, H. Liu, and S.-W. Yong, "Slow-wave half-mode substrate integrated waveguide using spoof surface plasmon polariton structure," *IEEE Trans. Microwave Theory Techn.*, vol. 66, no. 6, pp. 2946–2952, Jun. 2018.

[28] L. Ji, X.-C. Li, and J.-F. Mao, "Half-mode substrate integrated waveguide dispersion tailoring using 2.5-D spoof surface plasmon polaritons structure," *IEEE Trans. Microwave Theory Techn.*, vol. 68, no. 7, pp. 2539–2550, Jul. 2020.

[29] L. Ji, X.-C. Li, X. He, and J.-F. Mao, "A slow wave ridged half-mode substrate integrated waveguide with spoof surface plasmon polaritons," *IEEE Trans. Plasma Sci.*, vol. 49, no. 6, pp. 1818–1825, Jun. 2021.

[30] Y.-J. Guo, K.-D. Xu, X. Deng, X. Cheng, and Q. Chen, "Millimeter-wave on-chip bandpass filter based on spoof surface plasmon polaritons," *IEEE Electron Device Lett.*, vol. 41, no. 8, pp. 1165–1168, Aug. 2020.

[31] Y. Cui, K.-D. Xu, Y.-J. Guo, and Q. Chen, "Half-mode substrate integrated plasmonic waveguide for filter and diplexer designs," *J. Phys. D, Appl. Phys.*, vol. 55, no. 12, Mar. 2022, Art. no. 125104.

[32] X. Shen, T. J. Cui, D. Martin-Cano, and F. J. Garcia-Vidal, "Conformal surface plasmons propagating on ultrathin and flexible films," *Proc. Nat. Acad. Sci. USA*, vol. 110, no. 1, pp. 40–45, Jan. 2013, doi: 10.1073/pnas.1210417110.

[33] Z. Piatek, B. Baron, T. Szczegielniak, D. Kusiak, and A. Pasierbek, "Self inductance of long conductor of rectangular cross section," *Przeglad Elektrotechniczny*, vol. 88, no. 8, pp. 323–326, 2012.

[34] A. Kianinejad, Z. N. Chen, and C.-W. Qiu, "Design and modeling of spoof surface plasmon modes-based microwave slow-wave transmission line," *IEEE Trans. Microwave Theory Techn.*, vol. 63, no. 6, pp. 1817–1825, Jun. 2015.

[35] I. Savidis and E. G. Friedman, "Closed-form expressions of 3-D via resistance, inductance, and capacitance," *IEEE Trans. Electron Devices*, vol. 56, no. 9, pp. 1873–1881, Sep. 2009.

[36] M. Bozzi, L. Perregrini, and K. Wu, "Modeling of conductor, dielectric, and radiation losses in substrate integrated waveguide by the boundary integral-resonant mode expansion method," *IEEE Trans. Microwave Theory Techn.*, vol. 56, no. 12, pp. 3153–3161, Dec. 2008.

[37] Y. Zhou, Y. M. Huang, H. Jin, S. Ding, D. Xu, L. Silvestri, M. Bozzi, and L. Perregrini, "Slow-wave half-mode substrate integrated waveguide 3-dB Wilkinson power divider/combiner incorporating nonperiodic patterning," *IEEE Microwave Wireless Compon. Lett.*, vol. 28, no. 9, pp. 765–767, Sep. 2018.

[38] Y. Zhou, H. Jin, Y. M. Huang, S. Ding, D. Xu, N. Delmonte, M. Bozzi, and L. Perregrini, "An effective mixed extracting method for electromagnetic parameters of periodically loaded substrate integrated waveguide units and its applications," *IEEE Trans. Microwave Theory Techn.*, vol. 68, no. 2, pp. 543–554, Feb. 2020.

[39] A. Bharadwaj, A. Sharma, and C. C. Reddy, "An unconventional measurement technique to estimate power transfer efficiency in series–series resonant WPT system using S-parameters," *IEEE Trans. Instrum. Meas.*, vol. 71, pp. 1–9, 2022.

YUXI LIU was born in Huaian, China. He received the B.S. degree in electronic science and technology from Changzhou University, China, in 2019, and the M.S. degree in optical engineering from the Centre for Optical and Electromagnetic Research, South China Academy of Advanced Optoelectronics, South China Normal University, Guangzhou, China, in 2023. He is currently with Beijing Unigroup Tsingteng Microsystem Company Ltd. His current research interests include microwave components, leaky-wave antennas, and arrays.

YIMING ZHANG was born in Xianyang, China. He received the B.S. degree in electronic science and technology from Shaanxi University of Science and Technology, Xi'an, China, in 2016, and the M.S. degree in electromagnetic field and microwave technology from the Centre for Optical and Electromagnetic Research, South China Academy of Advanced Optoelectronics, South China Normal University, Guangzhou, China, in 2021. He is currently pursuing the Ph.D. degree with the Centre for Optical and Electromagnetic Research, Zhejiang University, Hangzhou, China. From 2021 to 2022, he was a RF Engineer with Xiaomi Communications Company Ltd., Shenzhen, China. His current research interests include microwave components, RF circuits, artificial intelligence-assisted design (AIAD), and microwave sensors.

HUI LIU (Member, IEEE) was born in Zhumadian, China. He received the M.S. degree in electromagnetic field and microwave technology from South China Normal University, China, in 2013, and the Ph.D. degree in microelectronics and solid state electronics from the Centre for Optical and Electromagnetic Research, Academy of Advanced Optoelectronics, South China Normal University, in 2018. From 2018 and 2020, he was a Postdoctoral Researcher with the Center for Optical and Electromagnetic Research, Zhejiang University. In 2020, he joined the School of Electronic and Information, Guangdong Polytechnic Normal University, as a Faculty Member. His research interests include antenna, RF circuits, and microwave components.

ERIK FORSBERG (Member, IEEE) received the M.Sc. degree in engineering physics and the Ph.D. degree in photonics from the Royal Institute of Technology (KTH), Sweden, in 1996 and 2003 respectively. He also studied business and economics at the Stockholm School of Economics, Sweden. During 2000, he was a Visiting Scientist at Hokkaido University, Japan, and a Post-Doctoral Fellow at KTH in 2003. He was a Faculty Member at Zhejiang University (ZJU), China, between 2004 and 2008. From 2009 to 2012, he was the Founding Graduate Dean (Associate) with the Higher Colleges of Technology (HCT), United Arab Emirates. In 2013, he rejoined ZJU as an Associate Professor. His current research interests include nano-lasers, plasmonics, and optical fiber devices.

SAILING HE (Fellow, IEEE) received the Licentiate and Ph.D. degrees in electromagnetic theory from the KTH Royal Institute of Technology, Stockholm, Sweden, in 1991 and 1992, respectively. He is currently a Professor with the Centre for Optical and Electromagnetic Research, Zhejiang University, China. He has been with the Department of Electromagnetic Engineering, KTH Royal Institute of Technology, as an Assistant Professor, an Associate Professor, and a Full Professor. He has first-authored one monograph (Oxford University Press) and has authored or co-authored more than 600 articles in refereed international journals. He has given many invited/plenary talks in international conferences, and has served in the leadership for many international conferences. His current research interests include electromagnetic metamaterials, optoelectronics, sensing, and communication.

● ● ●
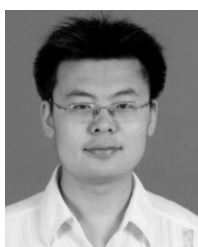
YUAN ZHANG was born in Shanxi, China, in 1980. He received the bachelor's and Ph.D. degrees in optical engineering from Beijing Institute of Technology, Beijing, China, in 2003 and 2009, respectively. Since then, he moved to Nanyang Technological University, Singapore, in 2009, and Zhejiang University, Zhejiang, China, in 2010, as a Postdoctoral Fellow. Since 2014, he has been a Faculty Member with the Centre for Optical and Electromagnetic Research, South China Normal University, Guangzhou, China. His research interests include metamaterials and artificial electromagnetic structures with interesting properties.